

Tunable plasmonic HfN nanoparticles and arrays

Sven H. C. Askes, Nick J. Schilder, Erwin Zoethout, Albert Polman, and Erik C. Garnett

Supporting information

Reactive sputter coating setup for HfN deposition	2
Optimization of HfN optical properties by ellipsometry.....	3
Drude model fit of the optical constants	4
UV-Vis-NIR optical spectroscopy	4
Rutherford Backscattering Spectrometry	5
Thin film roughness analysis using AFM	6
X-ray diffraction on HfN thin films	6
X-ray photoemission spectroscopy on HfN thin film.....	7
HfN nanoparticles made by FIB	8
FDTD simulations on HfN nanoparticles made by FIB-milling	9
Cathodoluminescence on HfN nanoparticles made by FIB milling.....	10
E-beam lithography preparation of HfN nanoparticles – Negative-tone resist.....	12
E-beam lithography preparation of HfN nanoparticles – Positive-tone resist	13
E-beam lithography preparation of HfN nanoparticles – Positive-tone triple-layer resist.....	15
Cathodoluminescence of HfN nanoparticles made by triple-layer EBL.....	18

Reactive sputter coating setup for HfN deposition

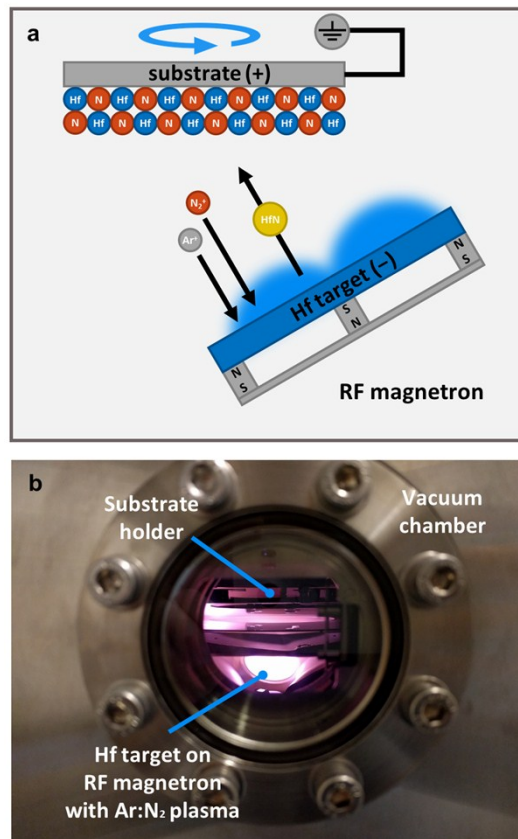


Figure S1. Reactive sputter coating setup used for deposition of HfN. a) Schematic illustration of the sputter coating process. Note the 35° angle of tilt of the RF magnetron with respect to the substrate holder. b) Photograph of inside the sputter coating setup vacuum chamber.

Optimization of HfN optical properties by ellipsometry

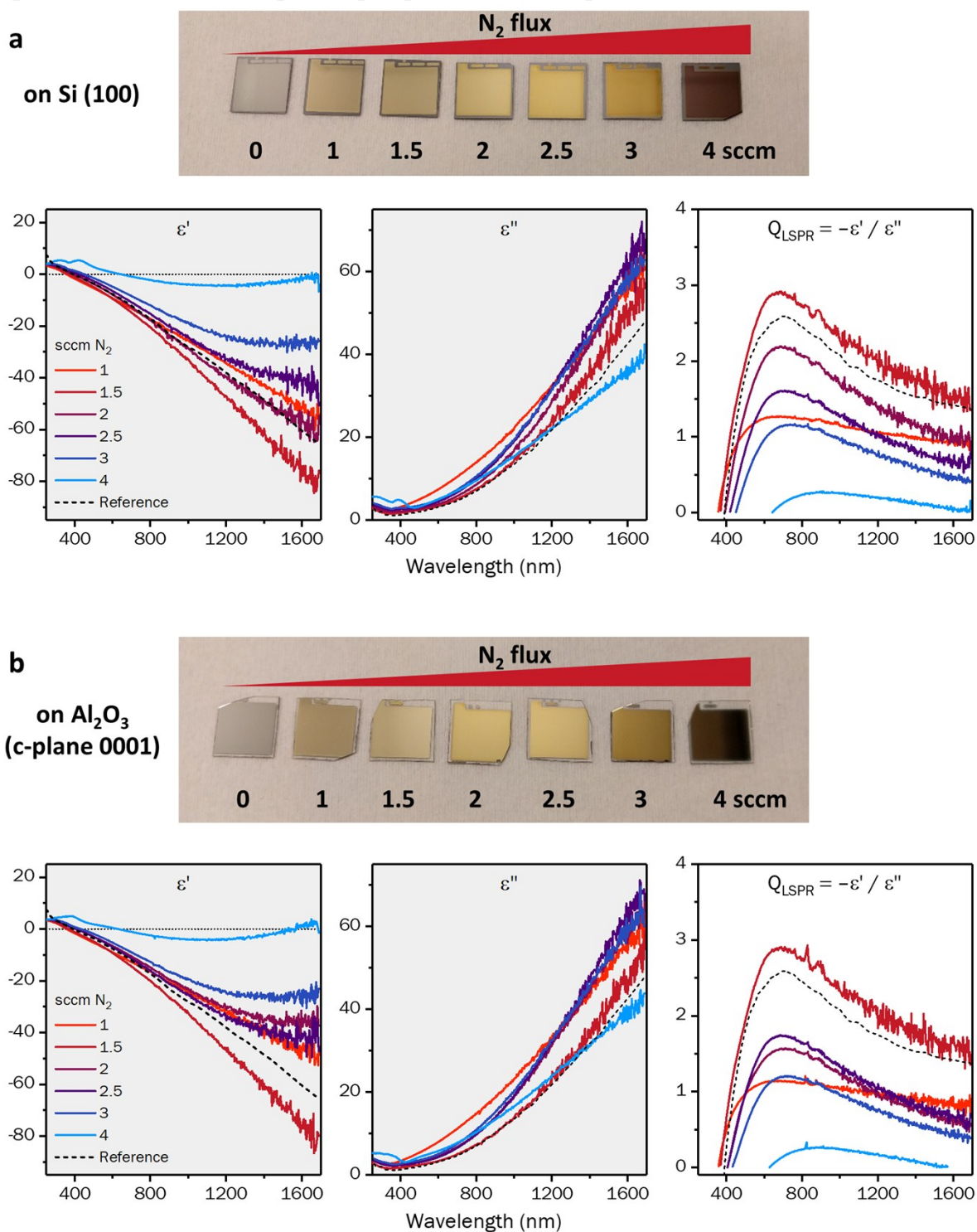


Figure S2. Real and imaginary parts of the dielectric permittivity and the LSPR quality factor ($Q_{\text{LSPR}} = -\epsilon' / \epsilon''$) of 200 nm HfN layers on Si(100) (panel a) and on c-plane Al₂O₃(0001) (panel b) for different nitrogen flows in the reactive sputter coater chamber. Optical constants were derived from ellipsometry. The total gas flow was kept at 36 sccm by adding Ar. Dashed lines indicate the data compiled by Ribbing and Roos (Handbook of Optical Constants of Solids, vol. 3, 1997, 351-369). **The HfN deposition with 1.5 sccm N₂ had the highest LSPR quality factor in the full spectral range and was therefore selected as best material for the preparation of HfN nanoparticles.** The brown color above 3 sccm N₂ flux indicates overstoichiometry (HfN_y, y>1), which was also confirmed by Rutherford Backscattering Spectrometry for a sample deposited at 3.5 sccm HfN (Figure S5).

Drude model fit of the optical constants

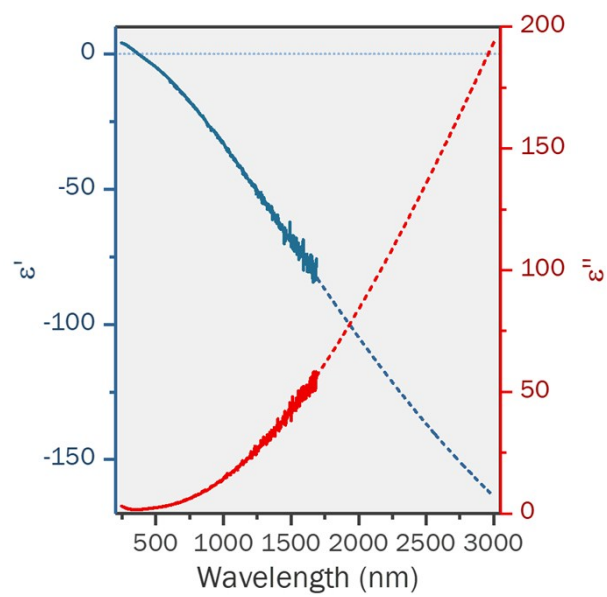


Figure S3. Real (blue) and imaginary part (red) of the dielectric constant of a HfN thin film (deposited at 1.5 sccm N_2 flux), fitted with a Drude model (dashed lines). The data was derived from ellipsometry. Drude model fit parameters: $\omega_\infty = 4.62$ eV, plasma frequency $\hbar\omega_p = 8.19$ eV; damping constant $\hbar\gamma = 0.48$ eV.

UV-Vis-NIR optical spectroscopy

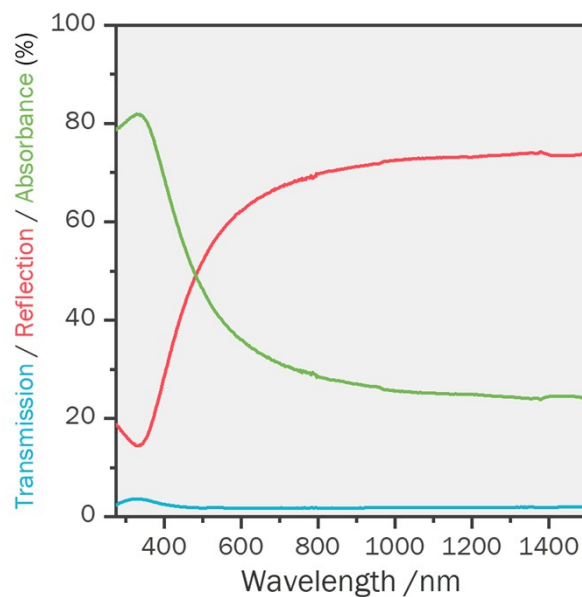


Figure S4. Transmission (blue), reflection (red), and absorbance (green) of a 88 nm thin HfN film deposited at 1.5 sccm N_2 flow.

Rutherford Backscattering Spectrometry

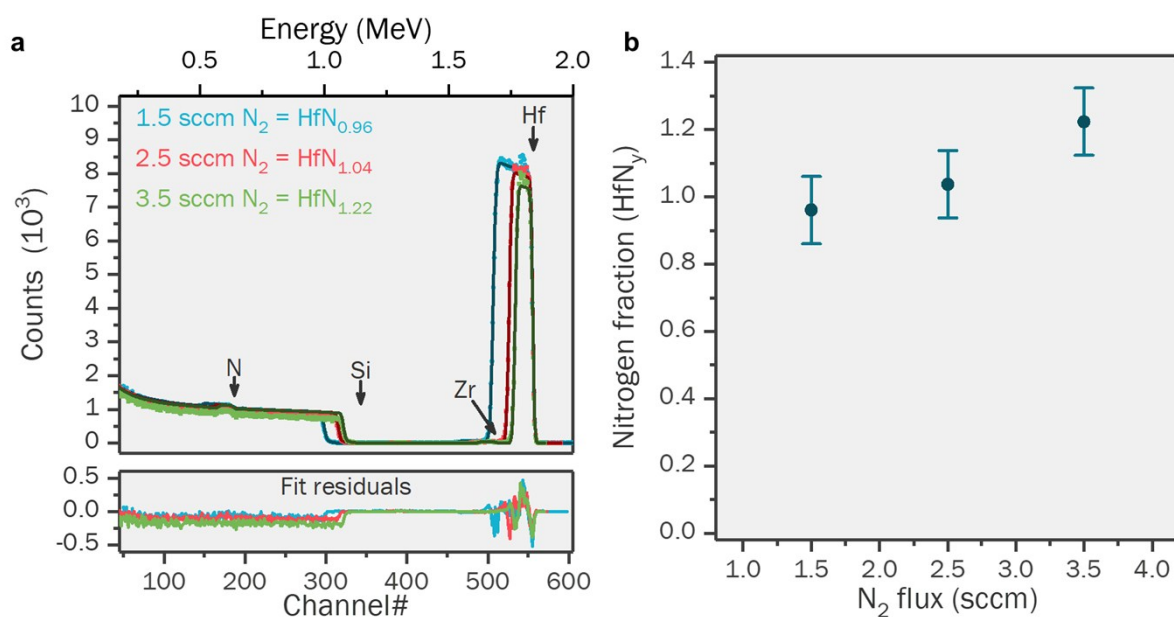


Figure S5. a) Rutherford Backscattering Spectrometry of three HfN thin films on Si substrate, deposited at 1.5 (blue), 2.5 (red), and 3.5 sccm N₂ flux (green). The data was fitted with SIMNRA software for RBS analysis and the extracted atomic nitrogen fraction (HfN_y) is given in panel b (blue data points). Error bars represent conservative estimates of the error due to lack of sensitivity to nitrogen (0.1 ratio units).

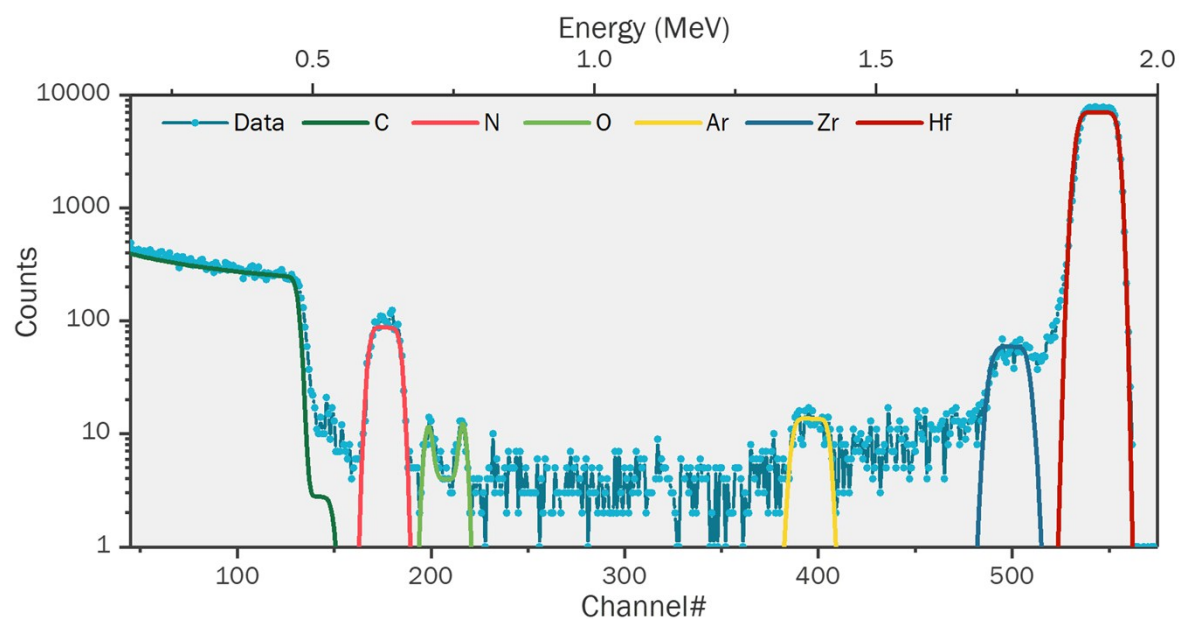


Figure S6. Rutherford Backscattering Spectrometry of a HfN thin films on Highly Ordered Pyrolytic Graphite (HOPG) substrate, deposited at 3.5 sccm N₂ flux (i.e. the atomic composition is HfN_{1.22}). Note the logarithmic scale of the y-axis. Tailing of the Hf signal was caused by substrate roughness. The HOPG substrate allows to observe the deconvoluted signal of light elements such as N and O. Argon and zirconium impurities were determined at 1.2 and 1.1 atom%, respectively. The oxygen concentration profile was best fitted with a ~1 nm HfO₂ top layer, less than 1.8 atom% oxygen in the HfN thin film bulk, and a ~1 nm HfO₂ bottom layer.

Thin film roughness analysis using AFM

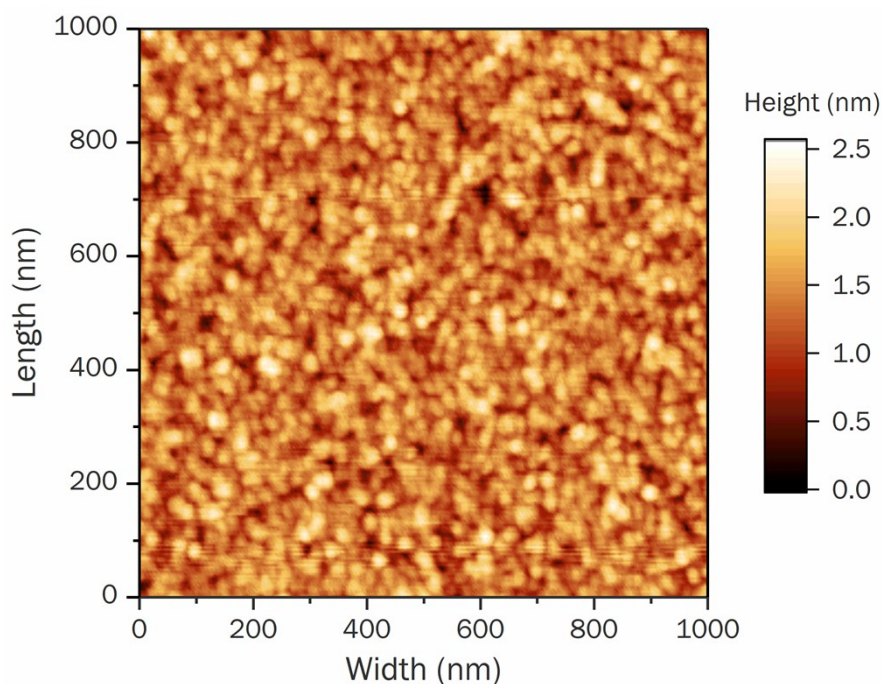


Figure S7. AFM height map of a HfN thin film on Si. The average RMS roughness was calculated to be 0.3 nm by use of Gwyddion AFM analysis software (D. Nečas, P. Klapetek, Cent. Eur. J. Phys. 2012, 10, 181, <http://gwyddion.net/>).

X-ray diffraction on HfN thin films

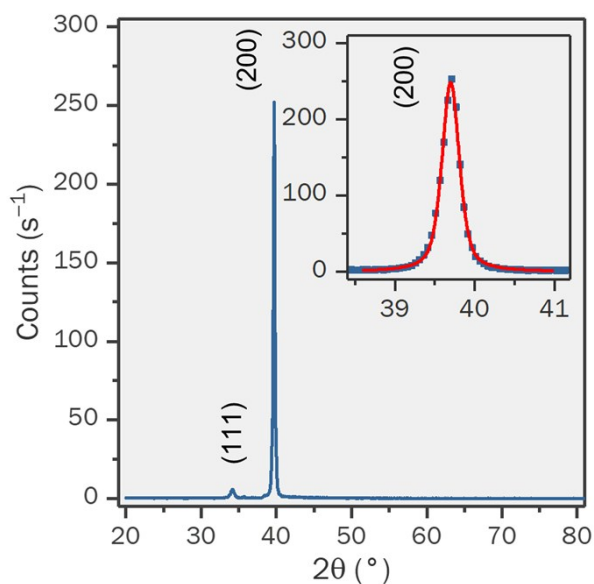


Figure S8. X-ray diffraction of HfN deposited with 1.5 sccm N₂ flow on c-plane sapphire. The (111) and (200) indices correspond to the reported diffraction pattern of cubic HfN with a lattice constant of 4.53 Å (R. Erwin, Metall. Mater. Trans. 1970, 1, 1249). The (200) peak at $2\theta = 39.7^\circ$ was fitted with a pseudo-Voigt function (red, $R^2 = 0.997$), from which the FWHM was determined to be 0.26° . After subtracting instrumental broadening (0.09°), the average crystallite size was calculated from the Scherrer equation ($\lambda = 0.15406$ nm), to be 47 nm.

X-ray photoemission spectroscopy on HfN thin film

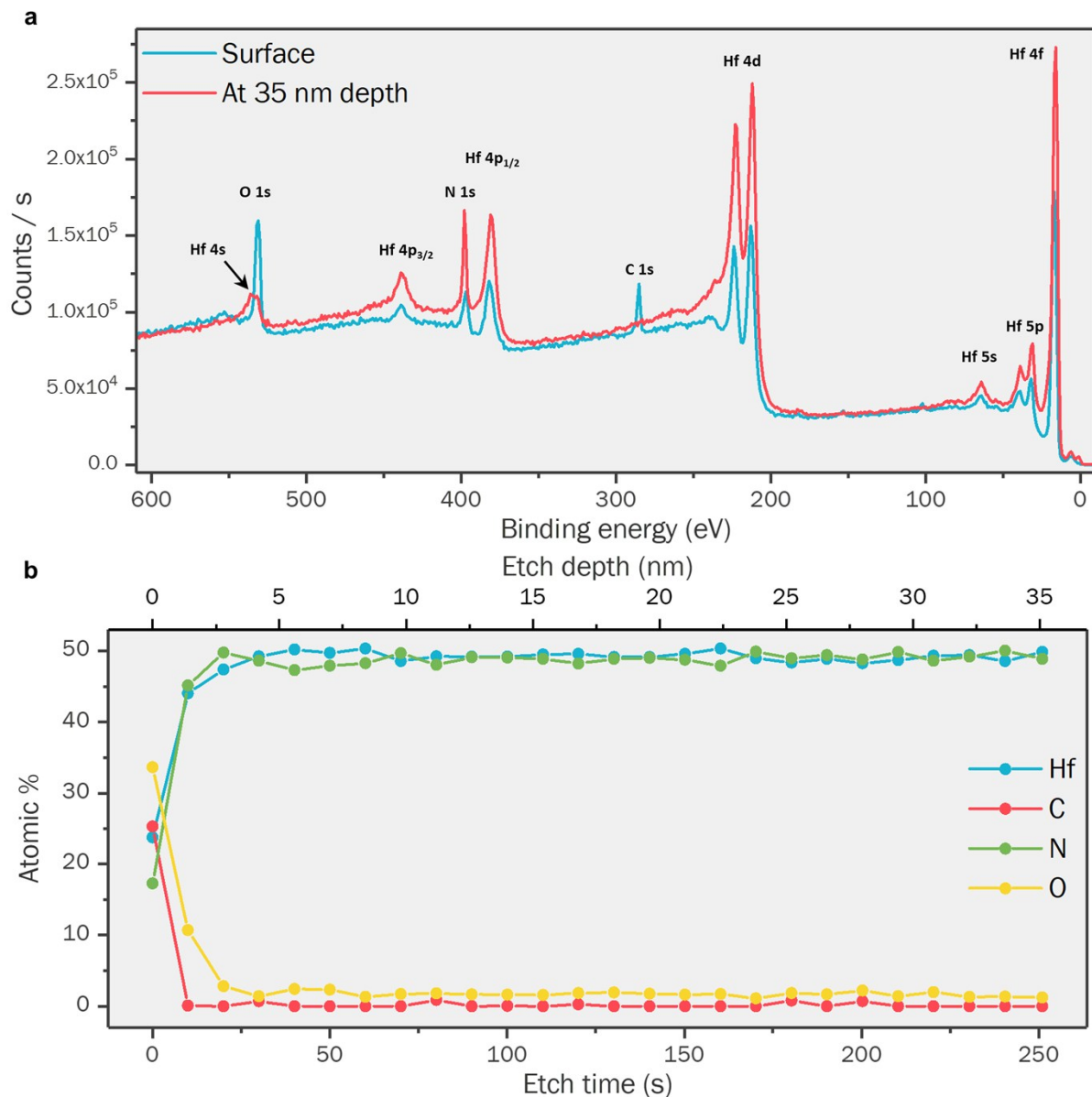


Figure S9. X-ray photoemission spectroscopy depth profiling of a HfN_{0.96} thin film. The spectrum closely matches those from literature. (A. Arranz; C. Palacio, Surf. Sci. Spectra 2006, 11, 33; A. J. Perry; L. Schlapbach, Solid State Commun. 1985, 56, 837.) a) XPS spectra at the surface (i.e. without etching, blue) and at 35 nm depth (red). After etching, note the disappearance of the C 1s peak at 285 eV and the great reduction of the O 1s peak. b) Atomic depth profile of the HfN thin film as a function of etch time. The HfN thin film was etched using Ar sputtering at a rate of 0.14 nm/s, and XPS spectra were taken each 10 s. Atomic percentages were calculated from spectral fitting of the Hf 4f, C 1s, N 1s, and O 1s regions. For the O 1s region, the Hf 4s and O 1s signals were deconvoluted. These data confirm the ~1:1 Hf:N stoichiometry and show the negligible incorporation of oxygen and carbon impurities.

HfN nanoparticles made by FIB

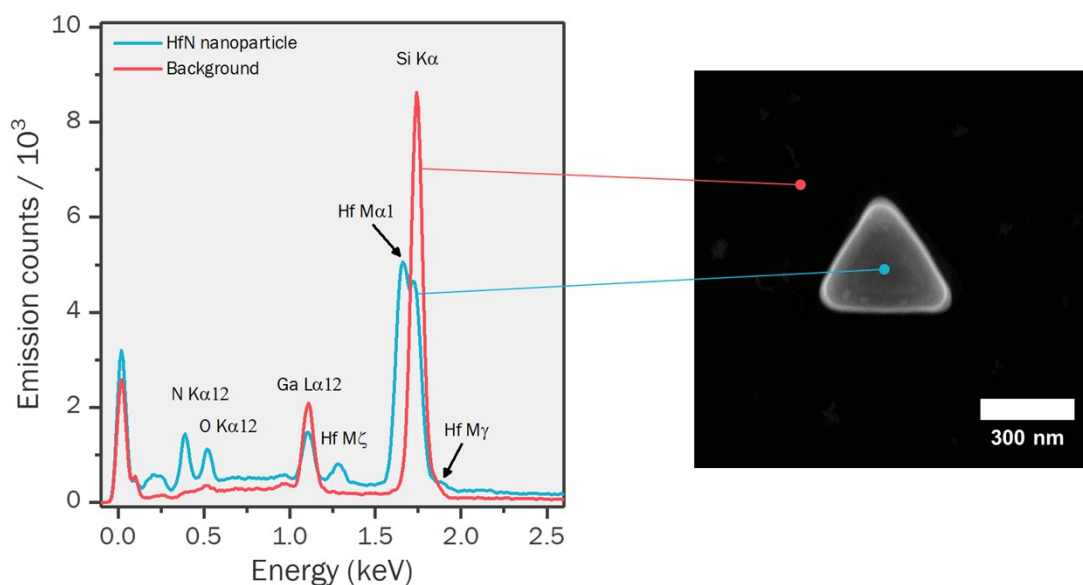


Figure S10. Energy dispersive X-ray spectrum of a region of a HfN nanotriangle prepared by focused ion beam milling (blue), and a spectrum of the background (red). Major X-ray emission lines are indicated.

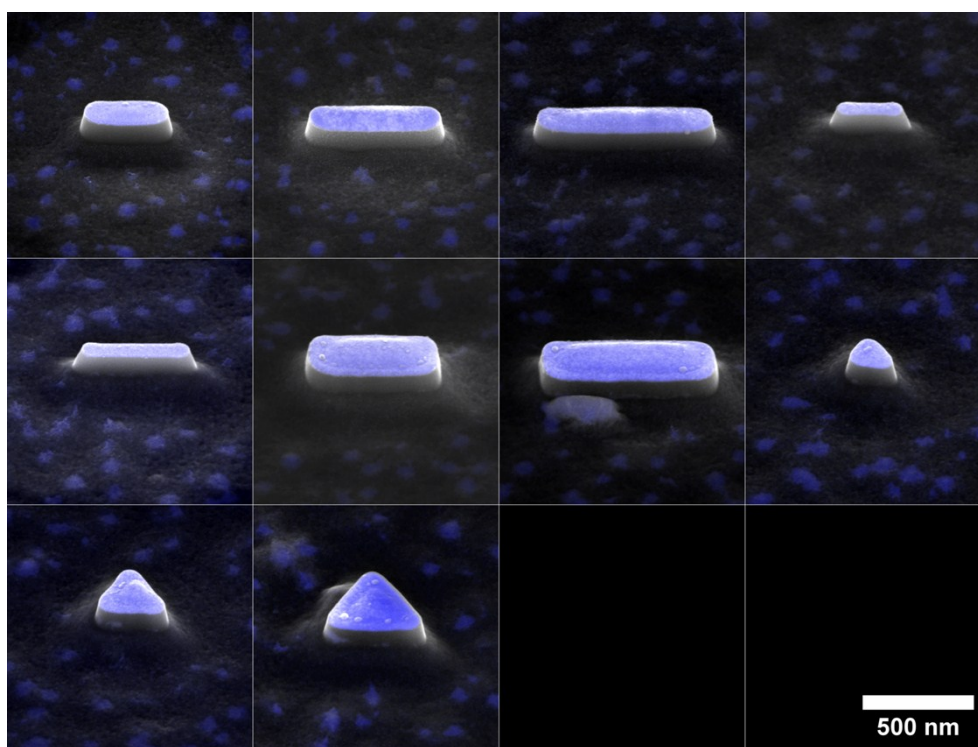


Figure S11. 45° tilted SEM images of HfN nanoparticles fabricated by focused ion beam (FIB) milling. The blue image overlay represents the backscattered electron image which reveals the location of heavy elements such as Hf. The combined images clarify that the HfN nanoparticles are supported on top of a shallow Si pillar.

FDTD simulations on HfN nanoparticles made by FIB-milling

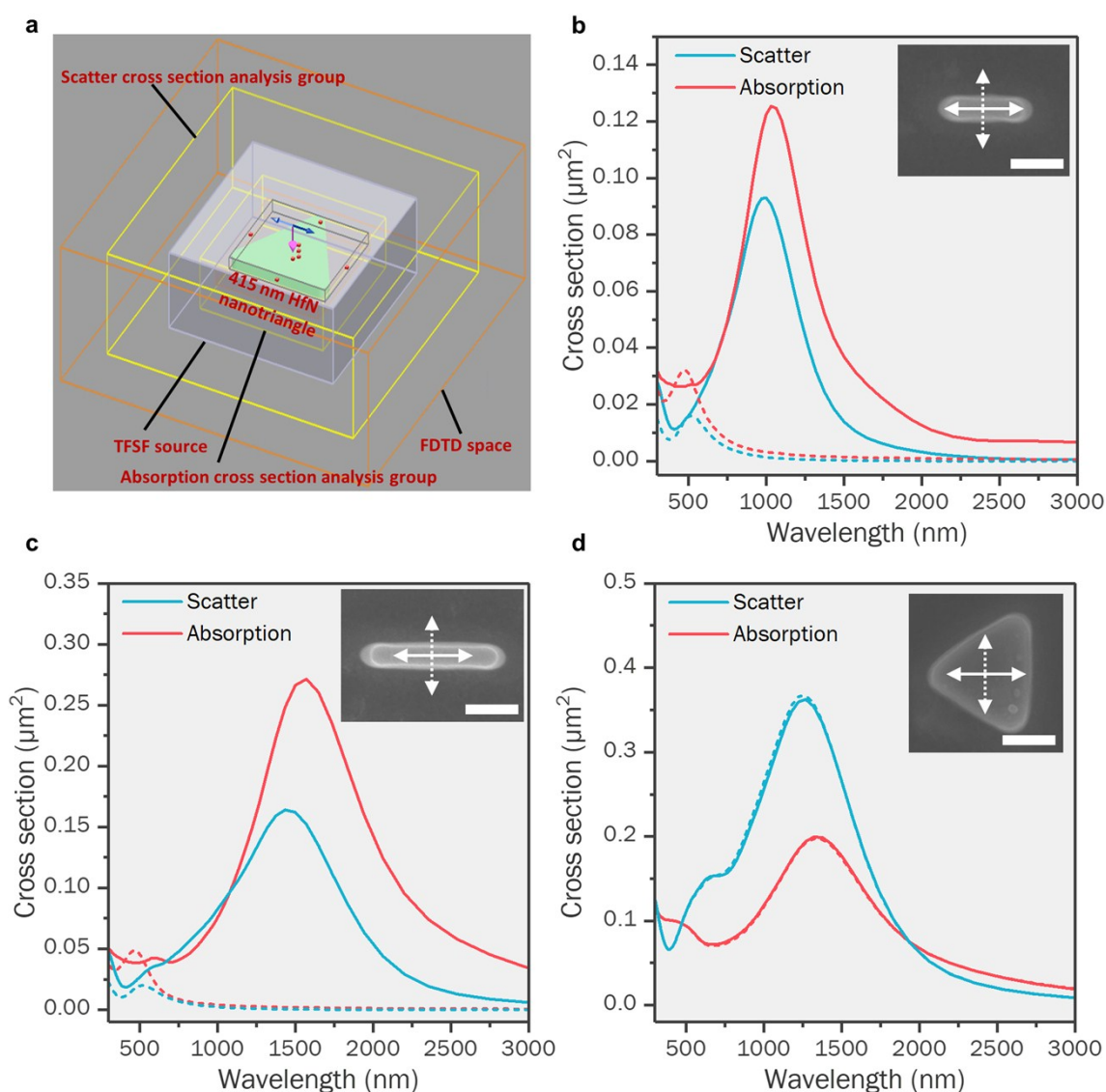


Figure S12. Finite-difference time-domain (FDTD) simulations using Lumerical software on HfN nanoparticles with dimensions equal to the structures made by FIB. a) Simulation geometry: The structures were approximated using xy-rounded polygons (35 nm curvature radius) with dimensions retrieved from SEM images, and the optical constants were taken from ellipsometry. A Total Field Scattered Field (TFSF) plane wave was used as light source with wavelengths of $\lambda = 300 - 3000$ nm and the absorption and scatter cross sections were evaluated using cross section analysis group boxes within the TFSF source box for absorption and outside the TFSF source box for scatter. The mesh size in the FDTD simulations was $5 \times 5 \times 5$ nm. The refractive index of the surrounding medium was set to 1. b-d) Scatter (blue) and absorption (red) cross section spectra for the three HfN nanoparticles shown in Figure 2, *i.e.* a 295×75 nm nanorod (b), 485×75 nm nanorod (c), and 415 nm equilateral triangle (d). Solid and dashed lines indicate longitudinal and transverse source polarization, respectively, as indicated with solid and dashed arrows in the inset SEM images. The scale bar is 200 nm for all three SEM images. The spectra of the nanorods consist of a transversal mode (around 500 nm) and a longitudinal mode (>1000 nm). CL spectra were obtained in the 370 – 730 nm wavelength domain, which indicates that only the high-frequency tail of the longitudinal plasmon modes were probed using CL. Note that infrared CL measurements ($\lambda > 1100$ nm) were not practical for these structures due to strong background luminescence from the silicon substrate in this wavelength domain.

Cathodoluminescence on HfN nanoparticles made by FIB milling

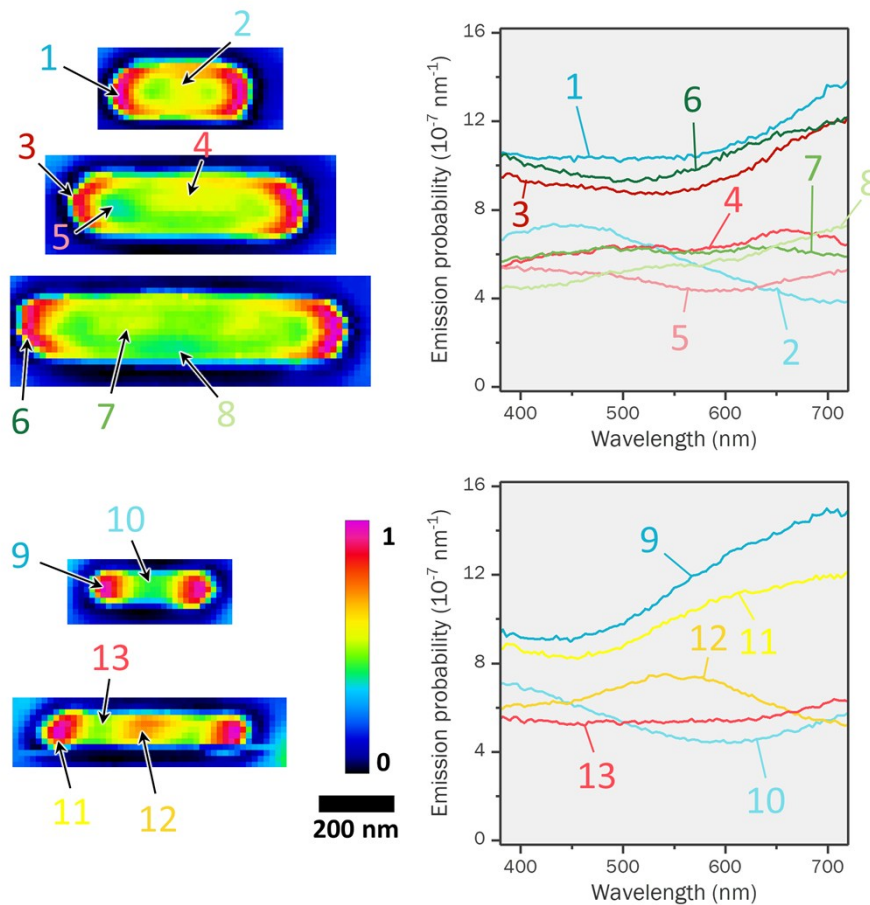


Figure S13. CL data of FIB-milled HfN nanorods. Left: CL intensity maps at $\lambda = 500 \pm 50$ nm, normalized to minimum and maximum values in each map. Right: CL emission spectra at the number-indicated locations.

Figure S13 shows the CL maps at $\lambda = 500 \pm 50$ nm and selected spectra of a variety of HfN nanorods. In the top three structures the nanorod width (W) is kept constant at 140 nm (wider than the 75 nm nanorods reported in the main text) and the length (L) is varied from 370 nm to 580 nm to 780 nm. For all three nanorods the emission intensity maximizes at the tips throughout the entire wavelength range, where the spectrum is very similar from structure to structure (compare spectra #1, #3, and #6). Interestingly, higher-order modes are observed for all three structures. For $L = 370$ nm, an antinode is localized in the center of the structure that corresponds to the second-harmonic resonance; at this location the spectrum maximizes at $\lambda = 450$ nm. For $L = 580$ nm, the antinode mode seems to be elongated and the spectral maximum is now at $\lambda = 650$ nm (spectrum #4). For $L = 780$ nm, two antinodes are observed that correspond to the third-harmonic resonance, but the spectrum (#7) no longer has a distinguishable emission maximum. The higher-order modes should also exhibit an emission maximum at the tips. However, contributions of the higher-order modes on the tip locations cannot be distinguished due to the broadness of the first-order contribution. The data of the lower two nanorods with $W = 75$ nm and $L = 295$ or 485 nm are discussed in the main text, with here also given the CL spectra at the resonance minima (spectra #10 and #13).

Figure S14 shows the CL maps at 500 ± 50 nm and selected spectra of two larger HfN nanorods with $W = 260$ nm and $L = 580$ and $L = 780$ nm and of three equilateral triangles with $W = 190$ nm, $W = 300$ nm and $W = 420$ nm. For the two large nanorods the emission maximizes at the four tips, which intensifies towards the NIR (spectra #14 and #17), but there are no distinguishable peaks in the observed wavelength range. These are first-harmonic modes that maximize in the NIR with

tailing through the visible range. We observe again higher harmonic modes (location/spectra #15 and #19, respectively) and they are better spatially and spectrally resolved than for their thinner counterparts in Figure S13 (top), with maximization of the resonance around $\lambda = 500 - 600$ nm.

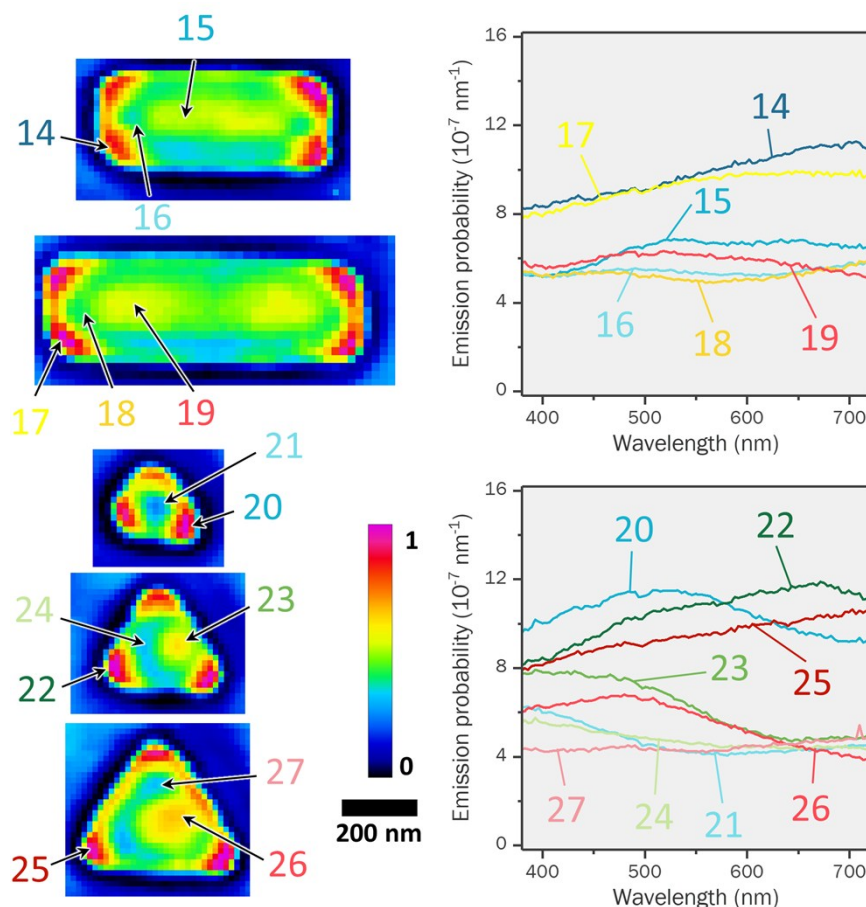


Figure S14. CL data of FIB-milled HfN nanorods and nanotriangles. Left: CL intensity maps at $\lambda = 500 \pm 50$ nm, normalized to minimum and maximum values in each map. Right: emission spectra at the number-indicated locations.

For all three nanotriangles we observe spatial resonance maxima at the tips, which maximize at $\lambda = 500$ and 650 nm for $W = 190$ and 300 nm, respectively. For the largest triangle the resonance maximum lies in the NIR, outside the observable spectrum. Meanwhile, when the triangle becomes larger, a central mode starts to appear. Whereas for $W = 190$ nm this central resonance is not observed in the visible range (spectrum #21), for $W = 300$ nm this resonance starts to appear and maximizes around $\lambda = 400$ nm (spectrum #23), and for $W = 420$ nm the maximum emission is observed around $\lambda = 500$ nm (spectrum #26). These observations are explained by the red-shifting of plasmon resonances as nanostructures get larger. For the largest triangle, at $\lambda = 500 \pm 50$ nm, some emission is also observed from the top two triangle sides which is not present for the middle triangle ($W = 300$ nm); this feature may be part of the higher-order resonance located in the center. Overall, these observations are consistent with plasmon modes in nanotriangles that were previously observed for Au/Ag nanotriangles (see main text), but are now also identified for a group-4 nitride material.

E-beam lithography preparation of HfN nanoparticles – Negative-tone resist

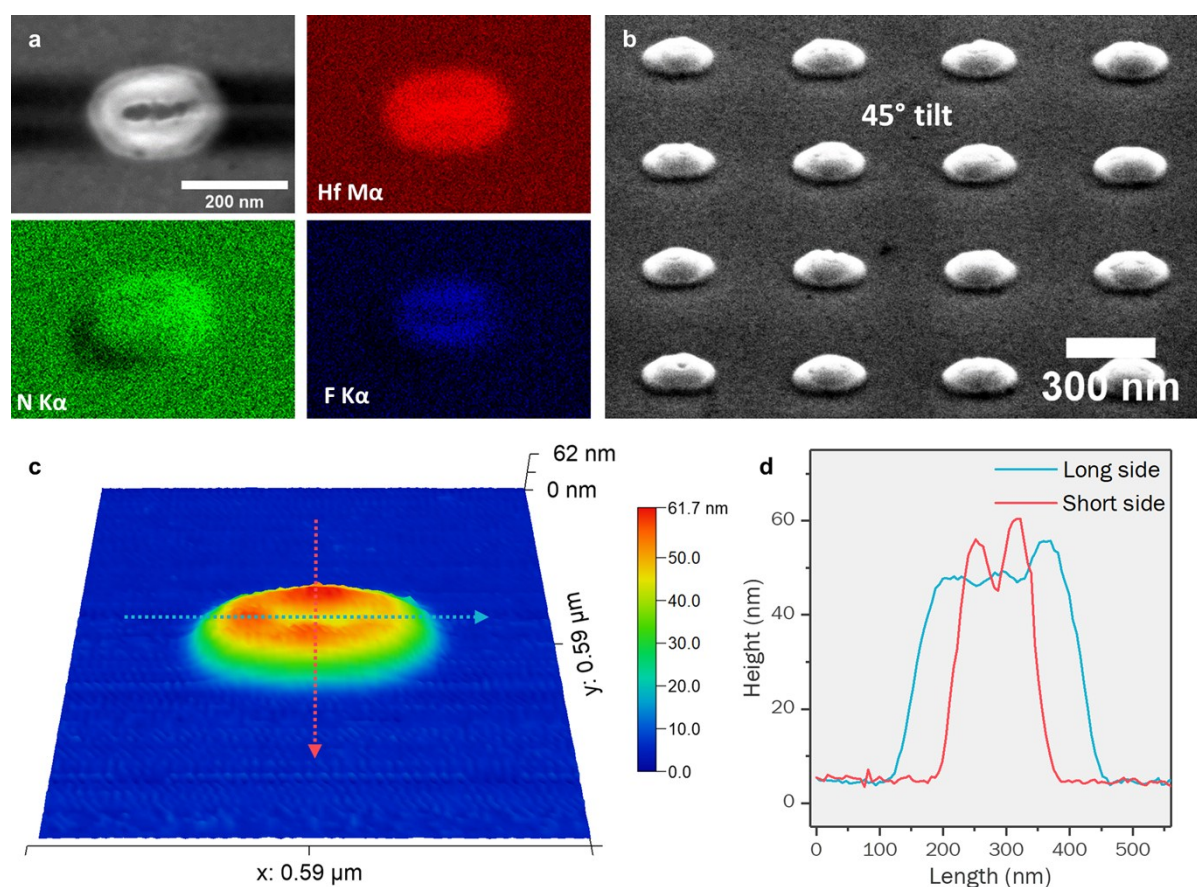


Figure S15. Characterization of HfN nanorods (180x60 nm rectangular design) made using negative-tone resist e-beam lithography. Experimental details for synthesis are given below. a) SEM and EDX with elemental maps of Hf (red), N (green), and F (blue). The background is due to a remaining thin film of HfN (~10 nm). The fluorine originates from elemental implantation during the etching procedure. b) SEM under 45° tilt. c&d) AFM 3D reconstruction (c) and AFM height profiles (d) along the x-axis (blue) and y-axis (red). Note the lack of sharp edges and the limited height of the particles, which discouraged further development of this approach.

Experimental details of negative-tone resist EBL

12 × 12 mm silicon (100) or sapphire (c-plane 0001) slides were coated with 65 nm HfN using reactive sputter coating at 500 °C. The slides were then prebaked at 150 °C for 1 min, spin coated at 4000 RPM for 45 sec (500 RPM/s acceleration) with 70 μL hydrogen silsesquioxane (HSQ, Dow Corning, XR-1541 6 wt.% in 4-methyl-2-pentanone), and baked at 180 °C for 1 min to yield a 120 – 140 nm resist layer. A 180 × 60 nm nanoparticle design was written in a matrix of 500 × 500 particles with a pitch of 500 nm using a Raith Voyager e-beam lithography system, operating at 50 kV. The structures were typically written with 2.2 nA beam current, 10 nm area step size, 900 ns dwell time, 11 mm/s writing speed, and 2.0 mC/cm² electron dose. The unexposed resist was removed by dipping the slides in tetramethylammonium hydroxide (25 wt.% in H₂O) at 50 °C for 60 seconds. Finally, the excess HfN was removed by reactive ion etching in an Oxford Plasmalab 80+ etcher using 300 W power and a mixture of 25 sccm Ar and 25 sccm SF₆ at 15 mTorr for 3.5 min.

E-beam lithography preparation of HfN nanoparticles – Positive-tone resist

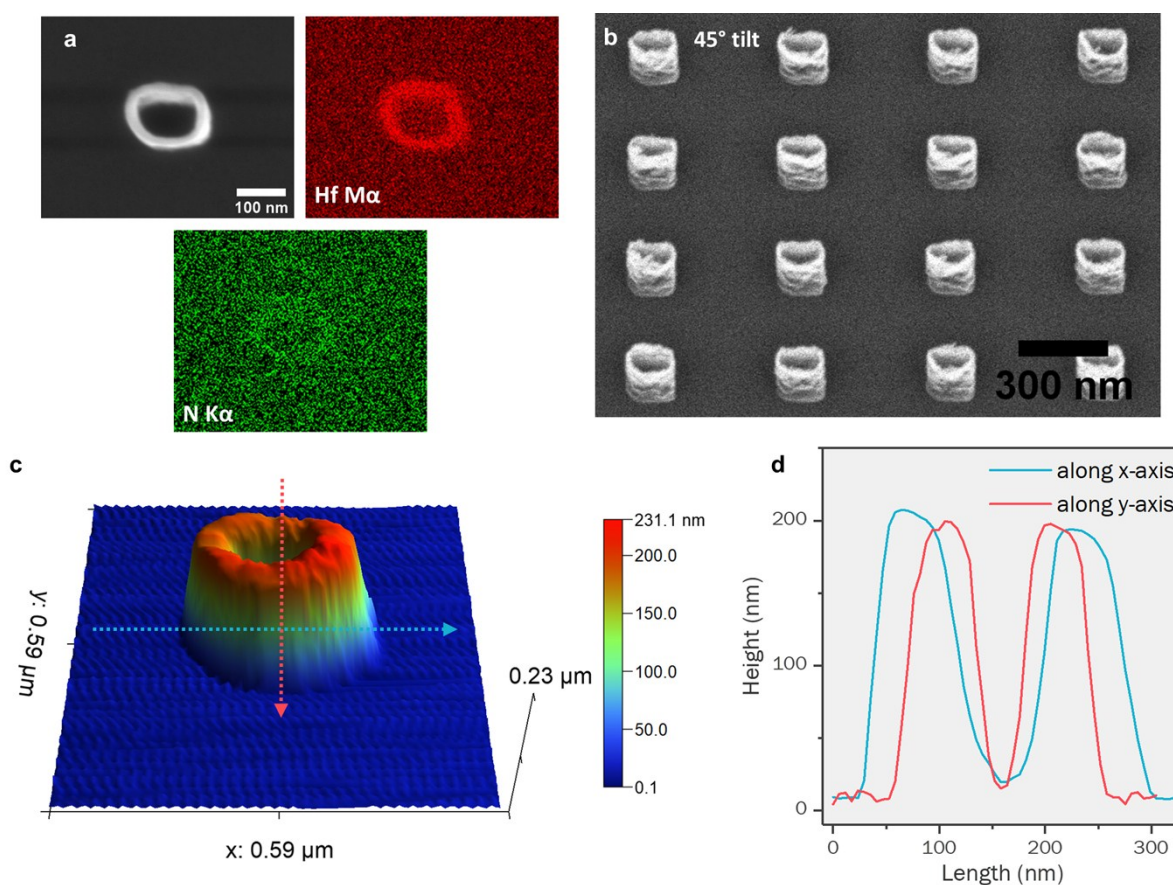


Figure S16. Characterization of HfN nanoparticles (120x60 nm rectangular design) made using one-layer positive-tone resist e-beam lithography. Experimental details for synthesis are given below. a) SEM and EDX with elemental maps of Hf (red), and N (green). Note that nitrogen yields a weak signal in EDX. b) SEM under 45° tilt. c/d) AFM 3D reconstruction (c) and extracted height profiles (d) along the x-axis (blue) and y-axis (red). Note the high and thin particle wall, made of poor-quality HfN (see Figure S17), and the negligible amount of material deposition in the middle of the particle.

Experimental details of single-layer positive-tone resist EBL

12 × 12 mm silicon (100) or sapphire (c-plane 0001) slides were prebaked for 1 min at 150 °C, spin coated at 3000 RPM for 45 seconds (1000 RPM/s acceleration, closed bowl) with 100 μL CSAR 62 (Allresist GmbH, AR-P 6200.13), and baked for 3 min at 150 °C to yield a 250 – 280 nm resist layer. In case of sapphire, an additional e-spacer was applied by spin coating at 4000 RPM for 60 seconds (1000 RPM/s acceleration, open bowl) with 100 μL Electra 92 (Allresist GmbH, AR-PC 5090), and baked at 90 °C for 2 min. A 120 × 60 nm rectangular nanoparticle design was written in a matrix of 500 × 500 particles with a pitch of 500 nm using a Raith Voyager e-beam lithography system, operating at 50 kV. The structures were written with 0.50 nA beam current, 10 nm area step size, 600 ns dwell time, 17 mm/s writing speed, and 0.30 mC/cm² electron dose. After writing, the sapphire slides were washed with H₂O for 60 seconds to remove the e-spacer, and dried with N₂. The exposed resist was removed through a sequential treatment with pentyl acetate (2.5 min), ortho-xylene (6 sec), 9:1 v/v methylisobutylketone:isopropanol (15 sec), and isopropanol (15 seconds), and were finally dried with nitrogen. A 65 nm HfN layer was deposited by reactive sputter coating at room temperature. Finally, the resist layer with excess HfN was lifted off by dipping the slides in anisole at room temperature for 60 seconds. No agitation by solvent flow or sonication was required during lift-off.

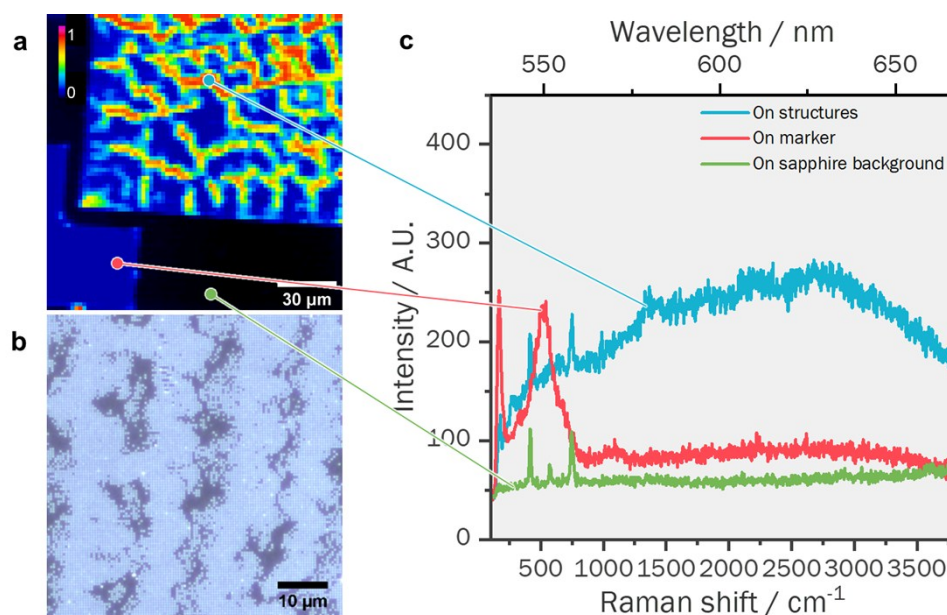


Figure S17. Raman/luminescence spectroscopy mapping of an array of HfN nanoparticles (120x60 nm design, 500 nm pitch square array) made using a one-layer positive-tone resist e-beam lithography. a) Normalized Raman intensity map of the total integrated spectral signal. b) Representative dark-field optical microscope image (on Si substrate). The black gaps in between the bright regions are areas without properly attached nanoparticles due to low lift-off yield. c) Raman/luminescence spectra at 532 nm excitation of the sapphire background (green), HfN marker (red), and the HfN nanoparticles (blue), indicated with arrows on panel (a). The characteristic phonon modes of HfN (Figure 1g) are visible on the marker, but not on the nanostructure array. Instead, the structures exhibit broadband luminescence, which we tentatively attribute to emission from a material combination of Hf, N, O, and/or C.

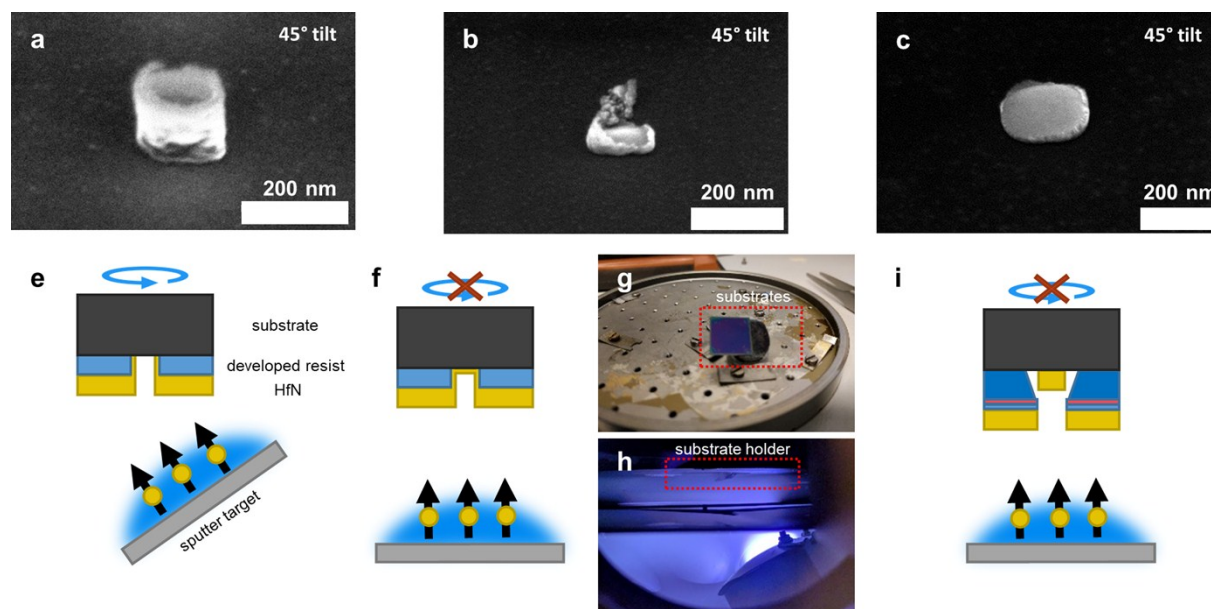


Figure S18. Positive resist strategy optimization showing the optimization of our e-beam lithography procedure. a,b,c) SEM images at 45° tilt of HfN nanoparticles made by different resist and deposition strategies, schematized in e, f and i, respectively. In the schematics, dark-grey layers indicate Si/Al₂O₃ substrates, yellow layers indicate deposited HfN, and blue layers in e and f indicate 500 nm CSAR 62 resist. The resist layers in panel i consist of 500 nm PMMA (top blue), 20 nm Ge (red), and 64 nm CSAR 62 (bottom

blue). g) Photograph of Si and sapphire patterned substrates (after the e-beam exposure step) on top of a 30° stub, on top of a substrate holder. h) Photograph of the same substrate holder, suspended bottom-up, during HfN sputter coating. The holder is rotated in the horizontal plane so that the substrates face the sputter target. In summary, the first strategy (a/e) resulted in the formation of poor-quality HfN hollow nanotubes, for which a negligible amount of HfN was deposited on the substrate. The second strategy (b/f) involved tilting the substrate with respect to the target, but the resulting structures still had significant HfN walls. The third strategy, for which a triple-layer resist undercut patterning was developed (see main text), was most successful in achieving deposition inside the e-beam patterned resist cavities while minimizing the formation of HfN walls in the final structure.

E-beam lithography preparation of HfN nanoparticles – Positive-tone triple-layer resist

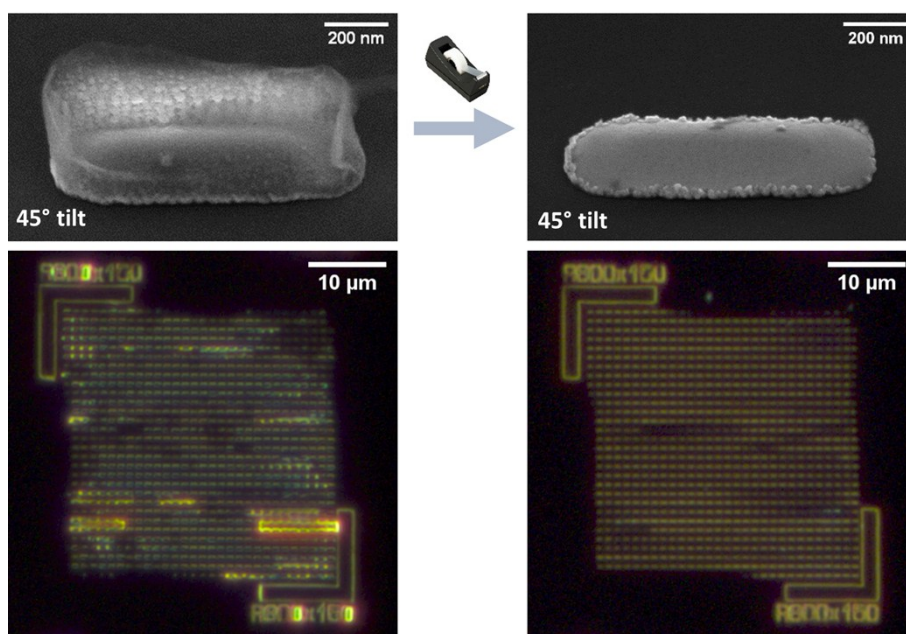


Figure S19. SEM at 45° angle (top) and dark-field optical micrographs (bottom) before (a) and after (b) tape exfoliation procedure on lithographically prepared HfN nanoparticles. Before tape treatment the HfN nanostructures have thin walls that scatter blue light. Also visible are parts of resist layers (yellow) that did not strip off during lift-off and sonication treatments. After tape treatment all of these imperfections have been stripped away at the bottom to leave a clean array of nanoparticles on the substrate.

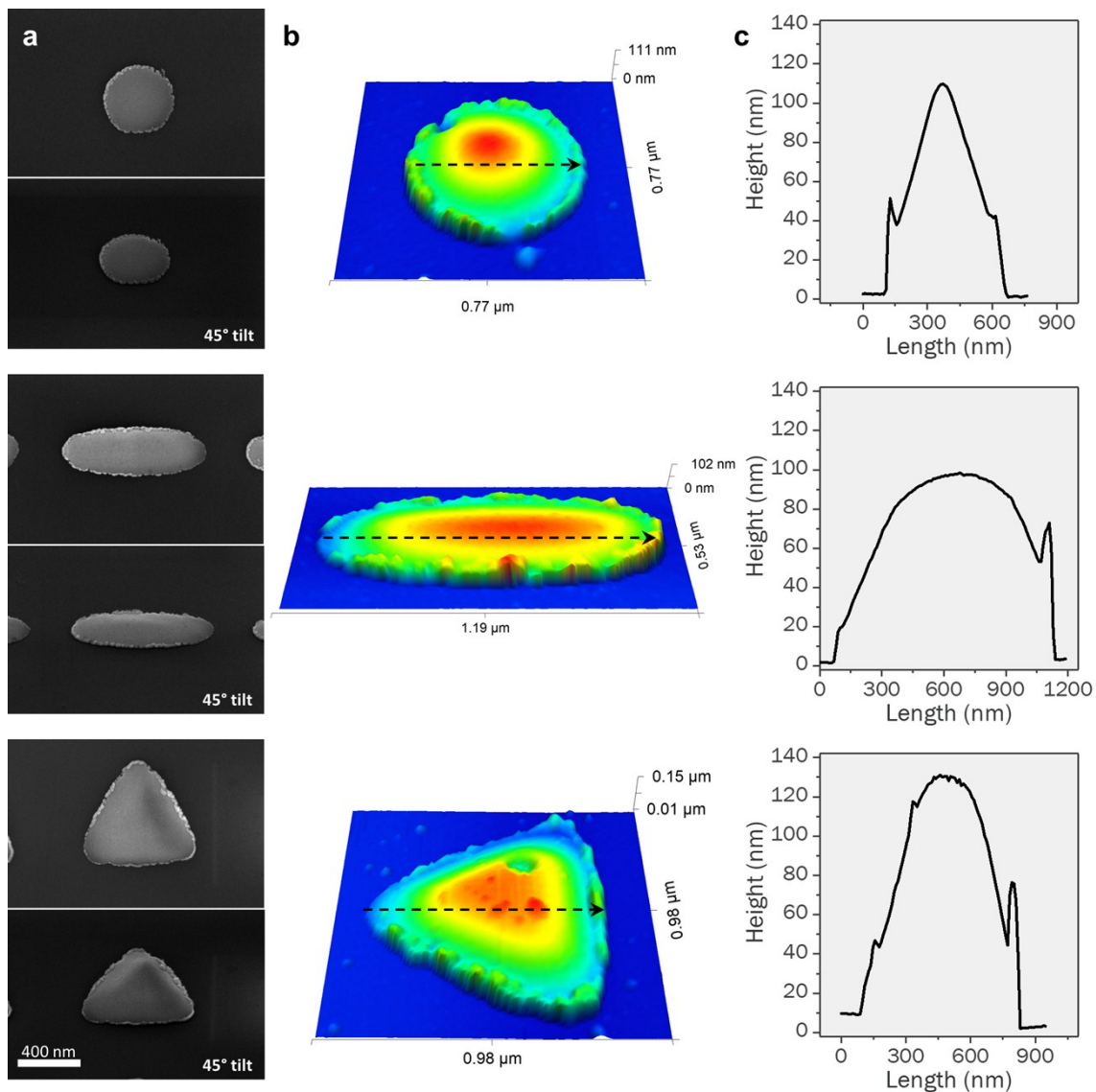


Figure S20. Various HfN nanoparticles fabricated through e-beam lithography. a) SEM images of the particles at 0° and 45° tilt. b) AFM 3D reconstructions of the particles shown in panels a and b viewed at 45°. c) Height profiles along the arrows indicated in b).

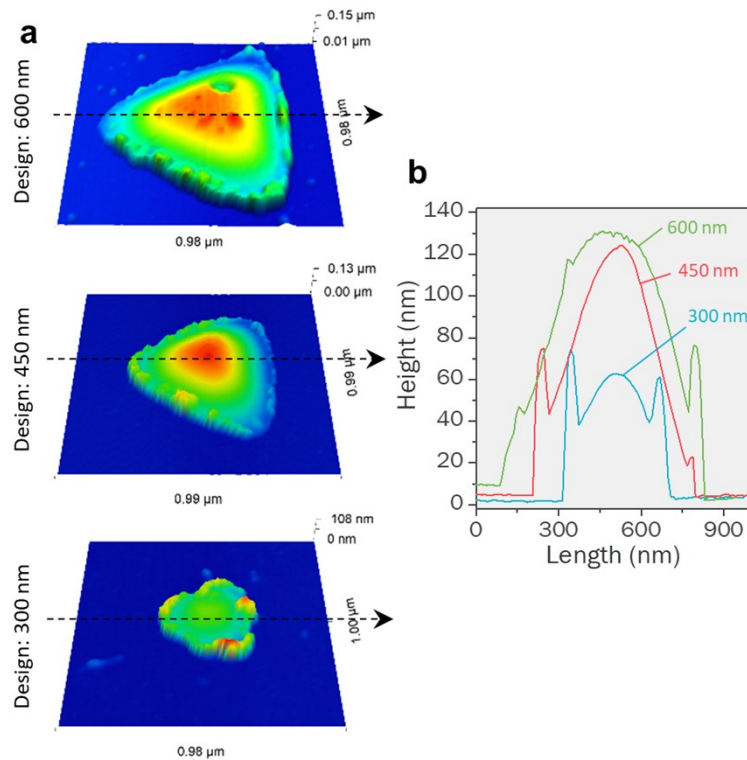


Figure S21. Comparison of differently sized equilateral HfN nanotriangles fabricated through e-beam lithography. a) AFM 3D reconstructions of triangles with a designed size of 600 nm (top), 450 nm (middle), and 300 nm (bottom). b) Extracted height profiles along the dashed arrows in panel a. Note how the 300 nm triangle is significantly lower in height than the other two.

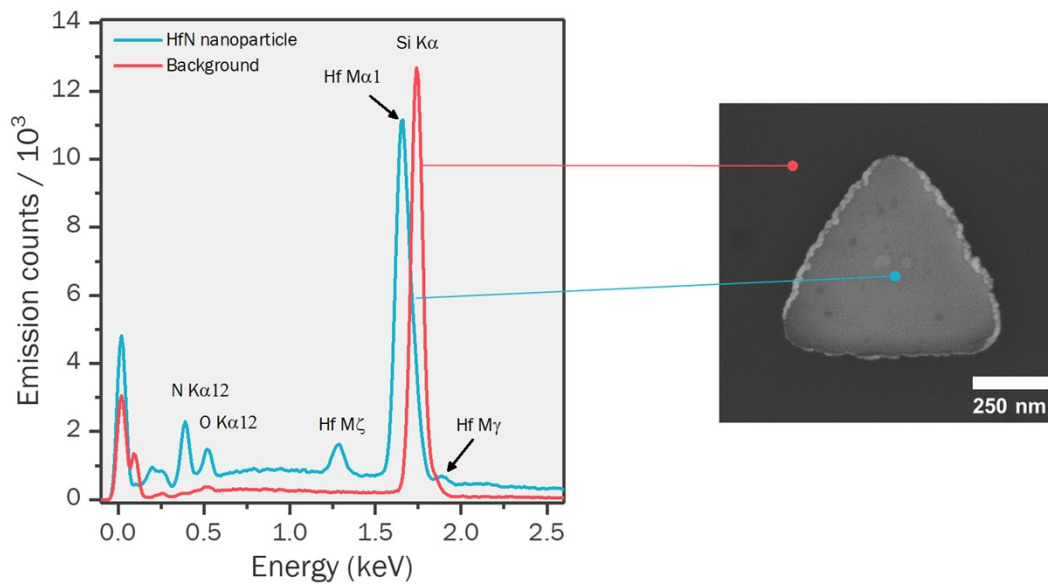


Figure S22. Energy dispersive X-ray spectrum of a region of a HfN nanotriangle prepared by positive-tone triple-layer EBL (blue), and a spectrum of the background (red). Major X-ray emission lines are indicated.

Cathodoluminescence of HfN nanoparticles made by triple-layer EBL

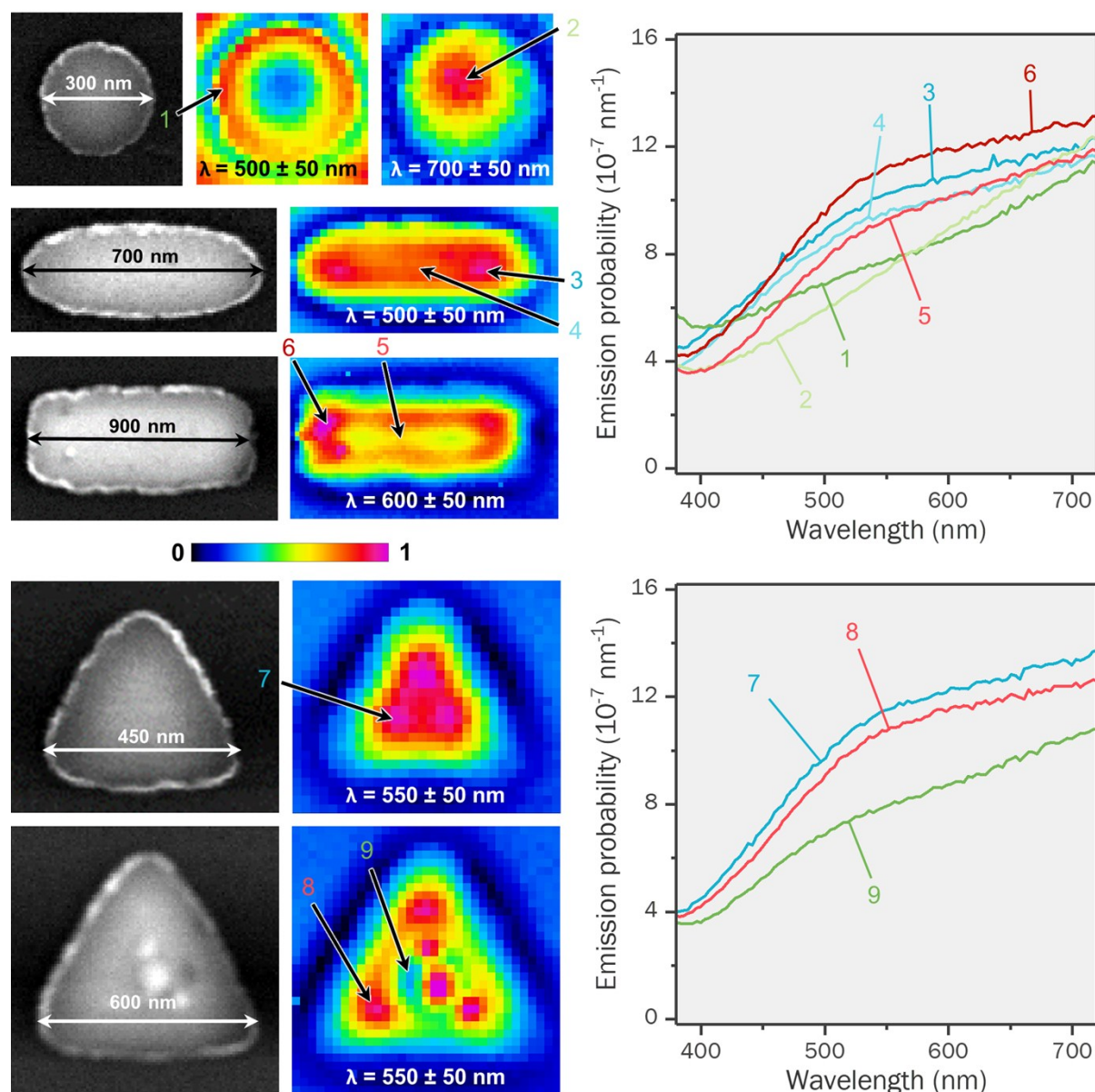


Figure S23. CL of EBL-fabricated HfN nanoparticles with varying shapes and dimensions. From top to bottom: 300 nm diameter disk, 700 × 150 nm ellipse, 900 × 300 nm rectangle, 450 nm triangle, and 600 nm triangle. The left column shows secondary electron images; the middle column shows normalized CL emission maps at the indicated wavelength ranges; the right column shows CL emission spectra at the locations indicated in the emission maps in the middle column.